

## Analysis of Thermoelectric Properties of Light Rare earth (La, Ce) Doped Nickel oxide Nanoparticles

Smita Jain<sup>1\*</sup>, Purnima Swarup<sup>1</sup>

<sup>1</sup>Department of physics, University institute of technology, Rajiv Gandhi Prodyogiki Vishwavidyalaya, Bhopal, India

Corresponding Author: Smita Jain

---

**Abstract:** The Nickel oxide (NiO) shows good characteristics for being used as an alternative material in high temperature applications and energy generation devices. In this work we study the doping effect on structural and thermoelectric properties of nickel oxide at the high temperature. In this work the temperature range for all the characterization is taken 900 K. Analysis was performed for all three samples using following techniques: i) Phase and Crystalline size determined by X-ray diffractometer (XRD) along with this Rietveld refinement also done by full profile fit ii) Fourier transform infrared spectroscopy (FTIR) for bond determination iii) morphology was observed by field effect-scanning electron microscope (FE-SEM) iv) thermal analysis was performed by Thermo gravimetric analyzer (TGA) and differential scanning calorimeter (DSC) and Laser flash analysis (LFA) v) Seebeck coefficient is calculated by the four probe method. The figure of merit of nickel oxide with various rare earth doping is found to be beneficial for the energy conversion at high temperatures. Nickel oxide (NiO) without doping and after doping with Lanthanum (NiO-La) and Cerium (NiO-Ce) shows some remarkable changes in their thermal and electrical characteristics thus it can be a better performing material for high temperature applications and also a good candidate for renewable energy conversion materials. From our analysis cerium doped nickel oxide (NiO-Ce) gave the highest figure of merit of about 0.08 at 900K which is much higher than previously established results.

**Keywords:** Rare earth, transition metal oxide, doped Nickel oxide, thermoelectric properties, semiconducting oxides.

---

Date of Submission: 01-03-2019

Date of acceptance: 18-03-2019

---

### I. Introduction

Transition metal oxides are extensively used materials in a wide variety of applications such as gas sensing, photo electronic and many more mechanical devices.[1,2] Nickel oxide (NiO) is most commonly used mono-oxide of this family, it shows semiconducting property at its nano level with band gap about 3.4 eV. It is a kind of functional material used in various electrical, thermal, optical and mechanical applications.[3,4] As we know that the properties of the materials are size dependent thus the nano size nickel mono oxide provides changes in their properties and shows attractive results. Doping in the materials also changes its basic characteristics and properties.[5,6] Many of the chemical physical and wet synthesis methods have been used for preparing the nickel oxide (NiO) nanoparticles, but all discussed methods have weaknesses especially their high cost and critical storage conditions ;[7-9] Among all the established methods we have chosen simple but effective method called combustion method.<sup>3</sup>

In this paper we have prepared pure nickel oxide (NiO), Lanthanum doped nickel oxide (NiO-La), Cerium doped nickel oxide (NiO-Ce) nanoparticles by combustion method. Rare earth materials are very good dopants and used most of the time as catalysts to revise the properties of the materials.[10,11] Doping of rare earth material enhances the various properties of the basic materials such as Dy, Pr & Nd improve the magnetization and use as the magnetic dopant for various applications, on the other hand Yttrium, cerium, Lanthanum and Holmium these are the materials which change the photoconductivity, thermal stability etc and uses in many sensing and mechanical devices.[12,13] The X-ray diffraction (XRD), scanning electron microscope (SEM) is done to determine the phase & morphology of the sample and Thermogravimetric analysis (TGA) and Differential scanning calorimeter (DSC) is being done for analyzing the change in thermal property due to rare earth doping.[3,14-16] Laser flash analysis (LFA) is used for thermal conductivity and four probe is used for Seebeck coefficient measurement and electrical conductivity measurement.

## II. Materials & Methods

Metallic precursors: Nickel nitrate hexahydrate {Ni (NO<sub>3</sub>)\*6H<sub>2</sub>O}[CDH India With 99.99 %purity], lanthanum nitrate hexahydrate{La(NO<sub>3</sub>)\*6H<sub>2</sub>O} [CDH India With 99.99 % purity], Cerium nitrate pentahydrate{Ce (NO<sub>3</sub>)\*5H<sub>2</sub>O} [CDH India With 99.99 % purity]

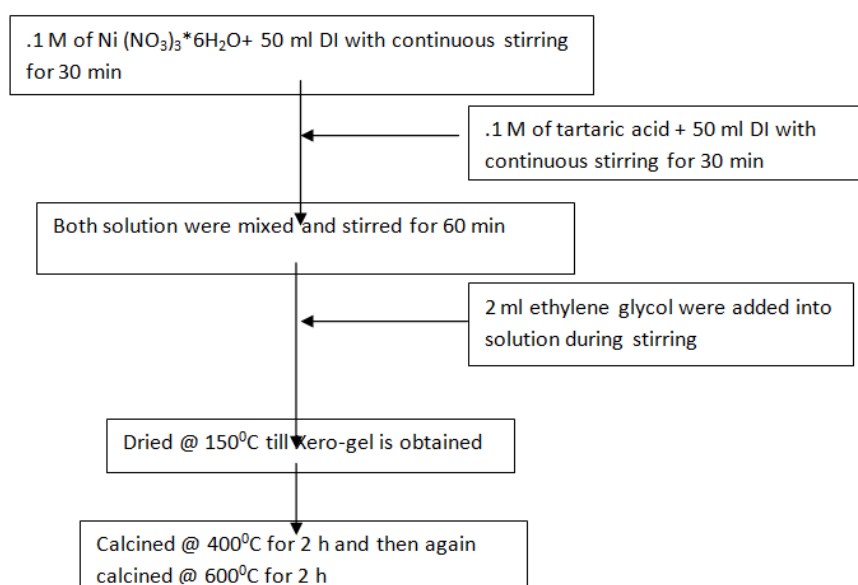
Solvent: De-ionized water

Ethylene glycol as capping agent, Tartaric acid (C<sub>4</sub>H<sub>6</sub>O<sub>6</sub>) for combustion.

For preparation of the material we can use sol gel combustion method.<sup>3</sup> The only difference in our opted method is that we can use water in place of ethanol and use tartaric acid in place of citric acid.

## III. Experimental Details

1 M of Nickel nitrate hexahydrate Ni (NO<sub>3</sub>)<sub>3</sub>\*6H<sub>2</sub>O (CDH India With 99.99 % purity) taking as metallic precursor dissolve in 50 ml de-ionized water with continuous stirring . On the other side tartaric acid (C<sub>4</sub>H<sub>6</sub>O<sub>6</sub>) also dissolve in 50 ml of de- ionized water (DI) with continuous stirring for 30 min in air atmosphere. Tartaric acid solution now added to the Nickel nitrate hexahydrate Ni (NO<sub>3</sub>)<sub>3</sub>\*6H<sub>2</sub>O solution and continuously stirred for 60 min. After an hour 2 ml Ethylene Glycol was added in the solution as polymerizing and capping agent and stirred for more 30 min under normal temperature and pressure condition. This prepared solution was dried at 150<sup>0</sup>C for 48 h for complete drying into xero-gel: this dried gel was crushed and calcined at 400<sup>0</sup>C for 2 h and again calcined at 600<sup>0</sup>C for 2 h in air atmosphere. This powdered sample is ready for further characterization. Flow-chart is given below;



## IV. Results and discussions

4.1 XRD analysis Fig. 1. Shows the Rietveld refinement of (a) pure NiO (b) NiO-La (c) NiO-Ce particles. The average crystalline size is being calculated by Debye-Sherr equation and tabulated in Table 1 while the rietveld refinement parameter has been listed in Table 2. The powder sample XRD shows the crystalline pattern and it is well matched with the standard JCPDS No. 04-0835 of Nickel oxide.<sup>3</sup> the observed angle 2θ at 37<sup>0</sup>, 43<sup>0</sup>, 62<sup>0</sup>, 75<sup>0</sup> & 79<sup>0</sup> represents the fcc phase. No impurity peaks has been observed in the above graph and all peaks are sharper and at higher intensity it means prepared material is well crystalline, while analyzing the doped NiO-La and NiO-Ce graph doping effect on the crystallinity of the material and size get also affected. All three samples are calcined at same temperature 600<sup>0</sup>c but the pure NiO is more crystalline than others. It is well established that at the temperature 600<sup>0</sup>C pure Nickel oxide shows optimum crystalline size but after doping its optimum calculation temperature for crystallinity were increases.[3,14]

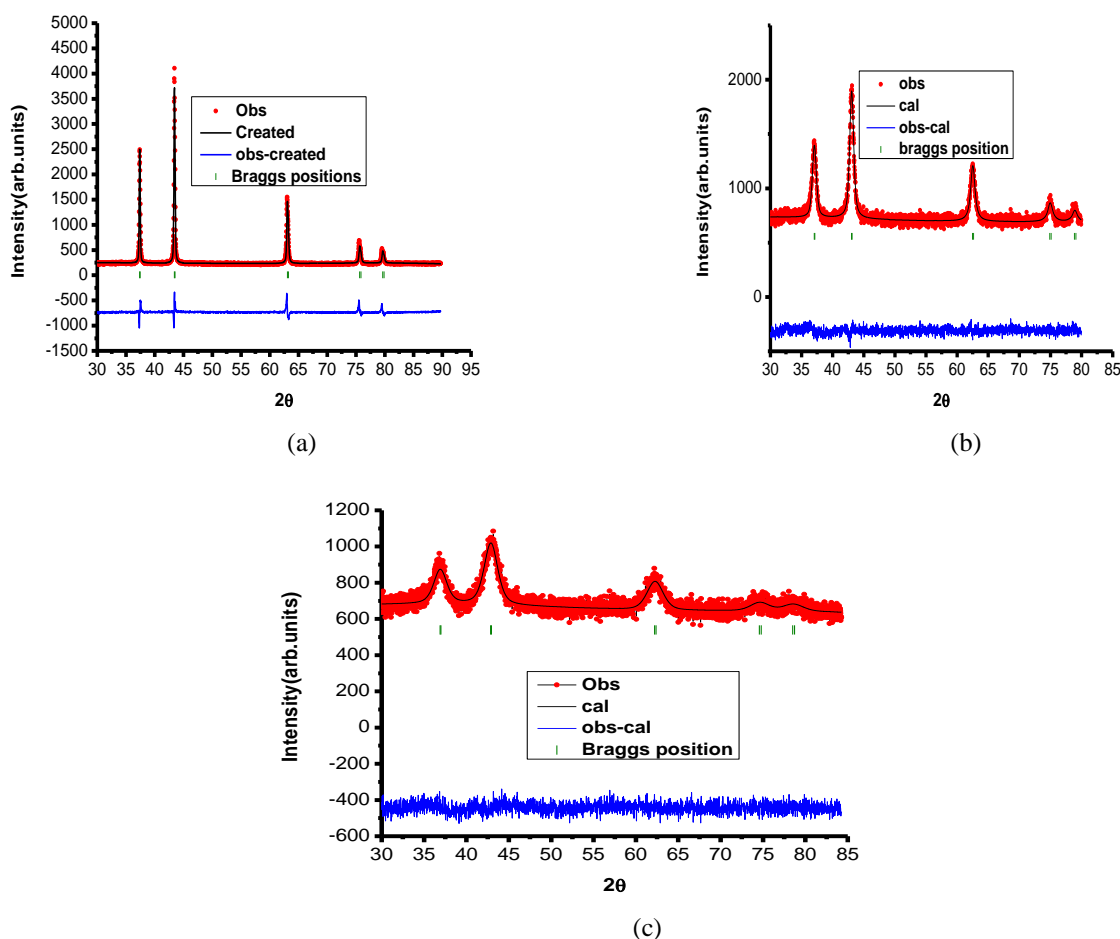


Figure 1. Rietveld refinement of (a) pure NiO (b) NiO-La (c) NiO-Ce.

Table 1 Average crystalline size of pure and doped NiO

2θ(degree)			θ (radian)			FWHM			β(radian)			Crystalline size (nm)		
NiO	NiO-La	NiO-Ce	NiO	NiO-La	NiO-Ce	NiO	NiO-La	NiO-Ce	NiO	NiO-La	NiO-Ce	NiO	NiO-La	NiO-Ce
37.20	37.2	36.9	.32	.315	.315	.37	.70	1.08	.0064	.012	.018	21.6	11.5	7.7
43.25	43.3	43.3	.37	.368	.368	.69	.647	1.56	.012	.011	.026	11.5	12.6	5.33
62.85	62.9	62.5	.54	.534	.534	.48	1.05	1.24	.0083	.018	.021	16.7	7.7	6.6
75.36			.65			.69			.012			11.5		
79.39			.69			1.08			.018			7.7		
Average crystalline size :-			NiO≈ 14 nm, NiO-La≈11nm, NiO-Ce≈7nm											

Table 2 Rietveld Refinement structural parameters for Pure and rare earth doped NiO nanoparticles

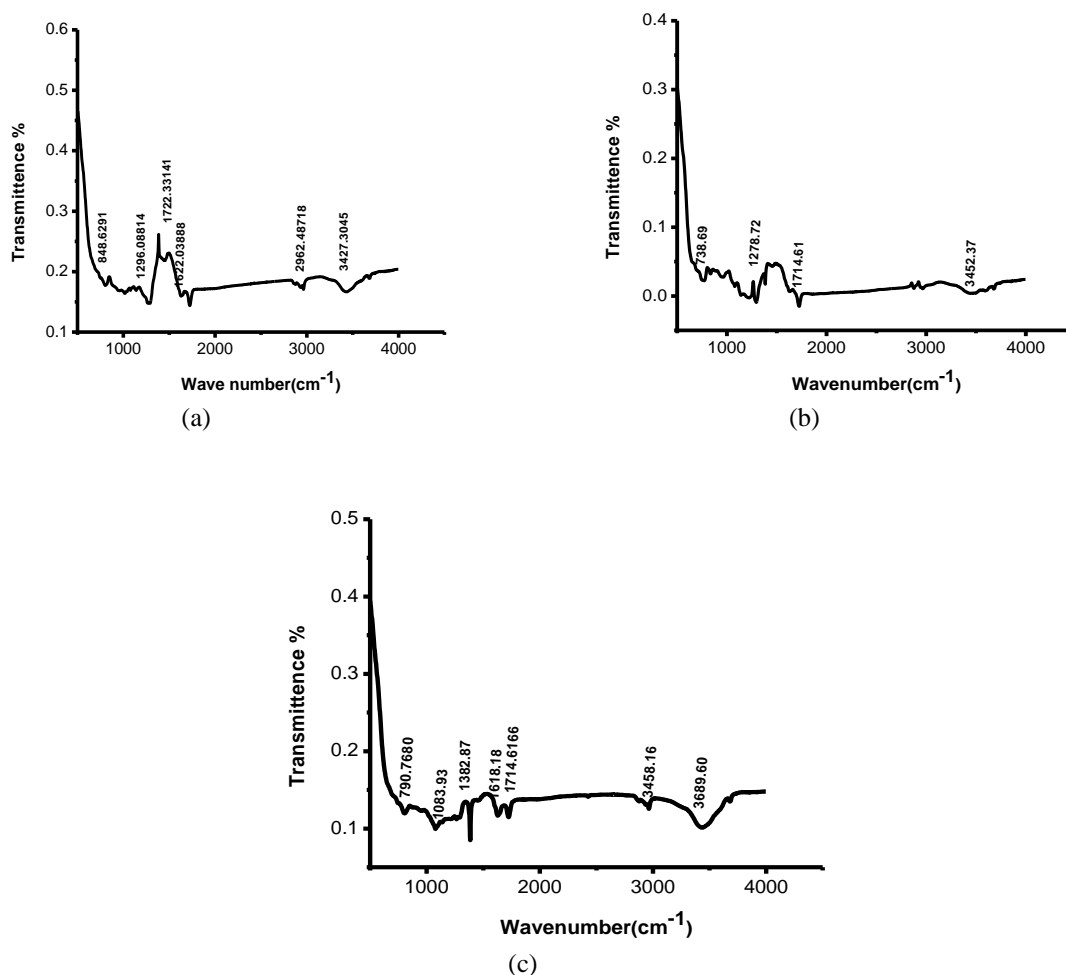
Space group: 225(F m 3 m) Structure: cubic

S.No	MATERIAL	U	V	W	a=b=c	occupancy	GOF	Chi <sup>2</sup>
1	NiO(SG)	.053908	.047862	.0067260	4.166	Ni=.9560, O=1.0051	1.285	1.66
2	NiO-La(SG)	1.9919	-1.735	.935462	4.20	Ni=.8382, O=1.01775	1.085	1.18
3	NiO-Ce(SG)	10.3515	-3.470	3.4351	4.21	Ni=.89455, O=1.0121	1.04	1.09

#### 4.2 FTIR results

Fig. 2. shows the FTIR spectra of the (a) pure NiO (b) NiO-La (c) NiO-Ce sample calcined at the temperature 400°C and sintered at the temperature 600°C. The IR spectrum of the above samples have many significant peaks over the range 4000 cm<sup>-1</sup> to 500 cm<sup>-1</sup>. The broad absorption band found in the range of 500-700 cm<sup>-1</sup> is assigned to Ni-O stretching vibration mode and absence of 3689 cm<sup>-1</sup> sharp peak respectively for the NiO, NiO-La due to anti-symmetric stretching vibrations in the Ni(OH) crystal structure further confirm that calcinating at 600°C for 2 hrs in air completely transform the hexagonal structure of Ni(OH) to cubic nanoparticles. However the peak at 3429 cm<sup>-1</sup> range shows some -OH might be linked with Ni as Ni(OH)<sub>2</sub>.

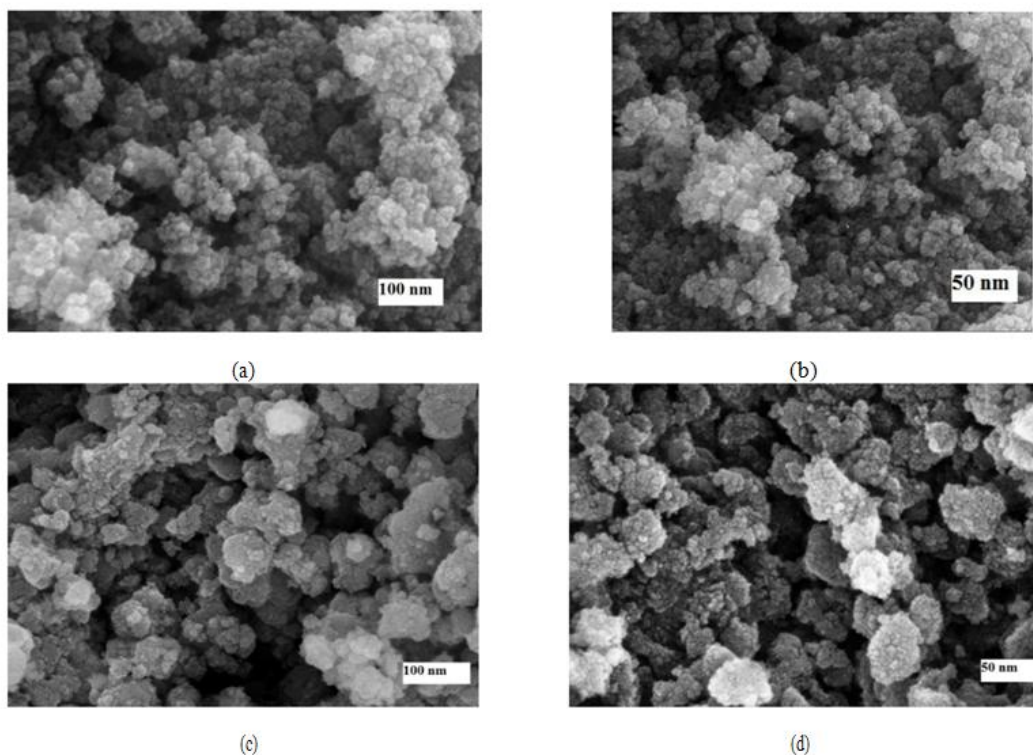
Peaks at 1100-1200  $\text{cm}^{-1}$  assigned to the C-O bond stretching vibration modes and the peaks near the region of 1300-1500  $\text{cm}^{-1}$  represents the absorption of Ethylene Glycol on Ni-O nanoparticles, some banding vibration modes of the H-O-H which indicates the presence of water traces in the samples. In our study pure NiO, NiO-La&NiO-Ce have these modes at the range 1622.038  $\text{cm}^{-1}$ , 1714.61  $\text{cm}^{-1}$  and 1618.18  $\text{cm}^{-1}$  respectively. The broadness of the band shows the nanocrystalline nature of the material. The peaks laying at 3200-3500  $\text{cm}^{-1}$  rang assigned to O-H starching vibrations and hydroxyl group occurs at 3400  $\text{cm}^{-1}$ . Thus by analyzing the plot we have seen that the prepared material is nanocrystalline and above three given samples the size of NiO-Ce is found to be in range of few nanometers.



**Figure 2.** FTIR spectrum of (a) pure NiO (b) NiO-La (c) NiO-Ce.

### 4.3 Morphology analysis

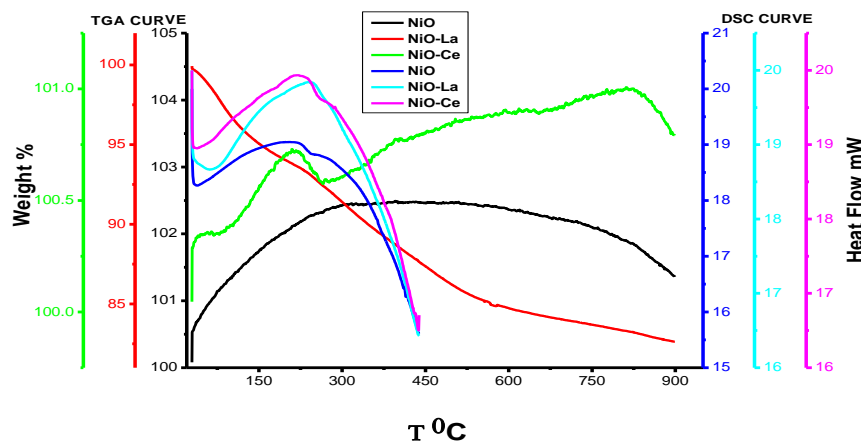
SEM; Fig.3(a), 3(b) shows the morphology of NiO-La at 100 nm & 50 nm respectively and 3(c) and 3(d) shows the morphology of NiO-Ce at 100 nm & 50 nm respectively. The sample were prepared in the same conditions and calcined at 400<sup>0</sup>C and 600<sup>0</sup>C the particles are shows spherical morphology.



**Figure 3.** Micrograph of (a) NiO-La 100 nm (b) NiO-La 50 nm (c) NiO-Ce 100 nm (d) NiO-Ce 50 nm

#### 4.4 Thermal analysis

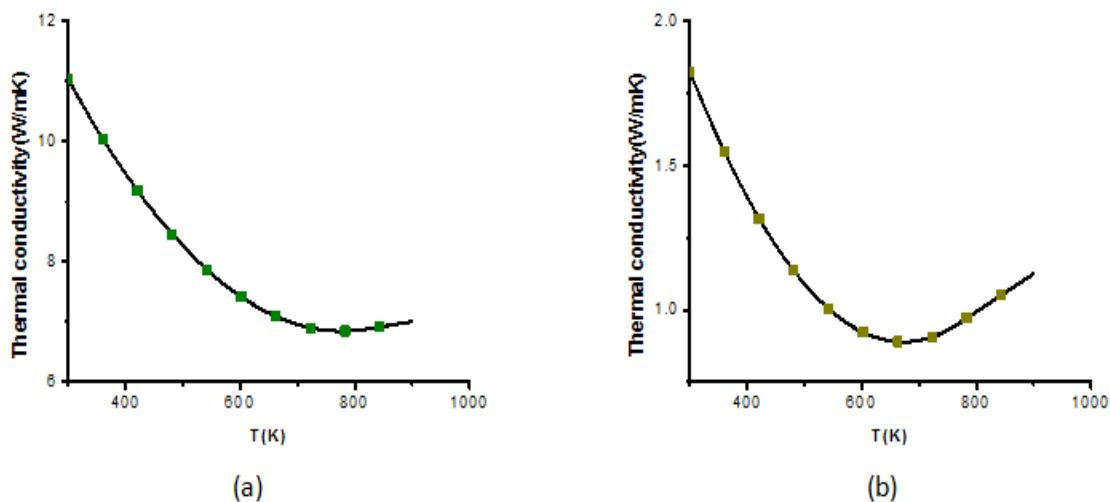
TGA & DSC curve analysis; Fig. 4. Shows the TGA/DSC pattern for the pure NiO, NiO-La and NiO-Ce respectively. All three samples were heated from room temperature at the rate  $10^{\circ}\text{C}/\text{min}$  up to  $900^{\circ}\text{C}$  in nitrogen atmosphere for TGA analysis and from room temperature to  $450^{\circ}\text{C}$  at the rate  $10^{\circ}\text{C}/\text{min}$  for DSC analysis. As the heating begins there is a small gain in mass of the pure NiO sample; this is due to sufficient purge process, and when the temperature reaches  $308^{\circ}\text{C}$  the maximum gain is observed, after this temperature a gradual loss in weight occurs due to the dehydration of the sample, which is in agreement with the heat flow curve of this sample. The DSC curve shows an endothermic loss of moisture and interlamellar water from a temperature of medium to approximately  $220^{\circ}\text{C}$  in all three samples. NiO-La shows gradual mass loss from the temperature  $68.20^{\circ}\text{C}$  and the maximum loss of about 17% occurred at the temperature  $560^{\circ}\text{C}$ , when maximum heat was generated from the sample, this mass loss stopped. The second endothermic peak was observed at  $433^{\circ}\text{C}$  due to the dehydration of the lattice hydroxyl group after calcination of NiO. It is noted that the first calcination temperature selected for NiO is  $400^{\circ}\text{C}$ . [15,16] On the other hand, the NiO-Ce curve was very unstable; a sharp peak of mass gain was observed in the curve at the temperature  $68.2^{\circ}\text{C}$ , which is very much similar to the pure NiO thermo-gram, but a slight decrease in mass was observed. As discussed before, the mass gain occurred due to sufficient purge process, but the fluctuations are the result of hydration and possible decomposition of the oxide material. The maximum mass gain was observed near the onset temperature of the heat flow curve; a sharp decrease in mass was observed after  $750^{\circ}\text{C}$ . It is known that the amount and microstructure of the defects also play an important role in the thermal stability of the materials. If the material consists of larger defects, it has lesser thermal stability. As shown in the figure, the prepared material is thermally unstable, meaning the sample has a large amount of defects and microstructures; this result also leads to the fact that the samples are in nanosize. [15,16] This was further supported by Laser flash analysis (LFA) of the samples, which provides the variation in thermal conductivity with respect to temperature.

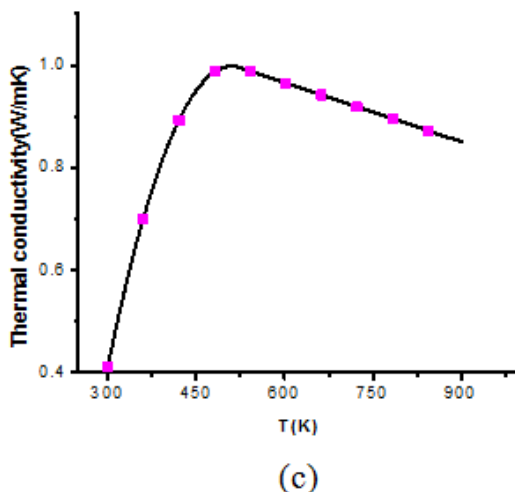


**Figure 4.** TGA/DSC curve of pure and doped NiO.

**4.5 Thermal conductivity:**

Fig. 5. Shows the thermal conductivity vs temperature graph of (a) pure NiO (b) NiO-La(c) NiO-Ce nanoparticles which were determined by LFA. These results are better correlate with the fact found in the DSC & TGA analysis that due to the defects the thermal stability of the material decreases. It is well established that thermal conductivity of oxide material is very low as compare to other composites so the prepared oxide material better correlated with this fact. As we have thermal conductivity of pure NiO nanoparticles is 7.008 W/mK at 900K and the value of Thermal conductivity of NiO-La nanoparticles is 1.257 W/mK at 900 K. The figure 5(a) and figure 5(b) depict that there is slight increment in thermal conductivity after certain temperature occurs in the samples due to the bipolar thermal conduction, this phenomenon mostly visible in semiconductor at high temperatures. As we know under normal circumstances the majority charge carriers dominate all the properties but as we increase the temperature the more and more minority charge carriers gets thermally agitated and hence contribution of minority charge carriers increases .[17-19] While figure 5(c) initially shows the increment in thermal conductivity from room temperature to up to 450 K after that it will show the gradual reduction in thermal conductivity due to thermal hysteresis, in which there is a phase transition occur.<sup>20</sup> Hence the material doped with the Cerium is better candidate of doping for reduction in thermal conductivity with value .85 W/ mK at 900 K.

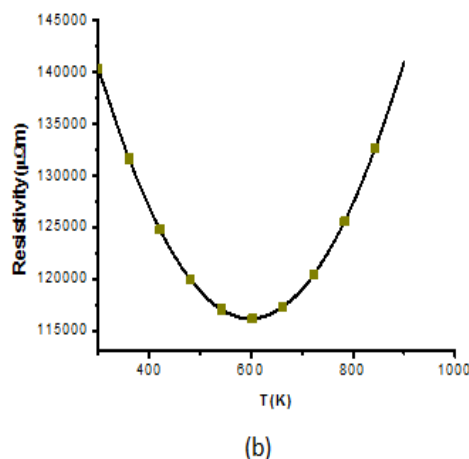
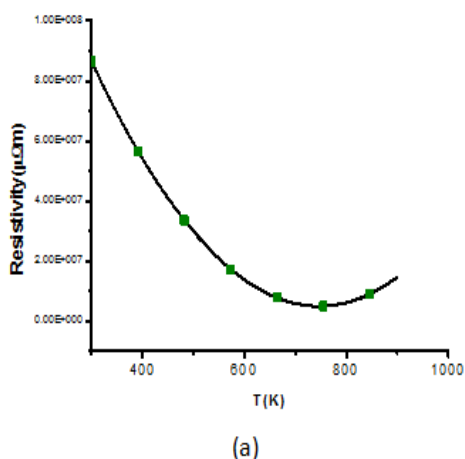




**Figure 5.** Thermal conductivity vs temperature graph of (a) Pure NiO (b) NiO-La (c) NiO-Ce.

**4.6 Electrical resistivity**

Fig. 6. depict that the electrical resistivity vs temperature graph of (a) pure NiO (b) NiO-La (c) NiO-Ce nanoparticles initially decreases as the temperature increases. In pure NiO after 650 K resistivity increases due to the thermal agitation which suppress the electronic conduction. In Figure 6(b) after 600 K resistivity increases and it shows continuous increment upto 900K this behavior is visible in semiconductors at high temperature regime.[21] as we know that extrinsic semiconductor always operated in the medium temperature range but if the temperature rise above to this range majority charge carriers gets thermally agitated and concentration of the charge carriers across the band gap is much larger than the doping concentrations. In this region holes concentration become equal to the electron concentration  $n_e = n_p$  due to this the mobility of majority charge carries decreases and hence resistivity increases.[22] But if we analyze the Figure 6(c) the resistivity of sample continuously decreases throughout the measured temperature range because of the preferential interface reduction. It is also observed that atomistic relaxation occurs at the interfaces and thus it eliminates many defects so the resistivity decreases in NiO-Ce nanoparticles with size and temperatures. [22]



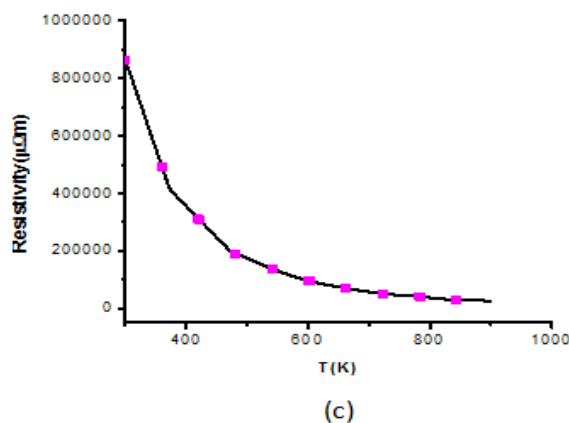


**Figure 6.** Electrical resistivity vs temperature graph of (a) Pure NiO (b) NiO-La (c) NiO-Ce

**4.7 Seebeck coefficient**

Fig. 7. Shows the Seebeck coefficient Vs temperature graph of (a) pure NiO (b) NiO-La (c) NiO-Ce nanoparticles which indicates that NiO-Ce had higher seebeck coefficient while NiO-La have very low Seebeck coefficient as compare with the pure nickel oxide. It is known that the material having higher positive Seebeck coefficient is semiconducting in nature thus the prepared samples are p-type semiconducting materials and used for thermoelectric properties study. If we analyze the plot characteristic it is observed that the Seebeck coefficient increased up to the 1000K and the cerium doped sample gives the highest increment in Seebeck coefficient it means NiO-Ce is a better candidate for thermoelectric applications. Plot clearly shows that due to bipolar thermal conduction seebeck coefficient is decreases as pure NiO has Seebeck coefficient 1170 μV/K at 900K whereas lanthanum doped nickel oxide(NiO-La) has Seebeck coefficient is around 105 μV/K at 900K which is very less as compare to pure and cerium doped nickel oxide(NiO-Ce). Cerium doped nickel oxide (NiO-Ce) has Seebeck coefficient 1390 μV/K at 900K.

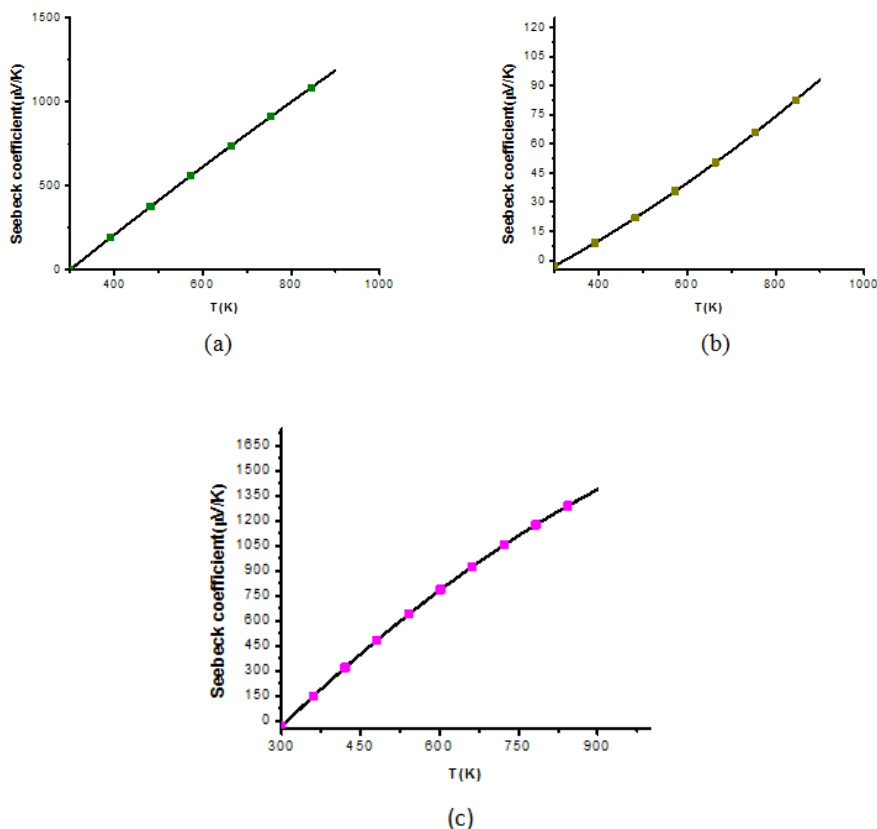


**Figure 7.** Seebeck coefficient Vs Temperature graph of (a) Pure NiO (b) NiO-La (c) NiO-Ce.

**4.8 Figure of merit (ZT)**

Fig. 8. Shows the figure of merit vs temperature graph of (a) Pure NiO(b) NiO-La (c) NiO-Ce nanoparticles, this parameter is being calculated by the help of above determined parameters such as thermal conductivity, electrical resistivity and Seebeck coefficient by putting them in the formula:

$$ZT = (S^2/\rho k) T, \tag{1}$$

ZT is a dimensionless quantity. By the above formula the calculated figure of merit of the Pure NiO, NiO-La and NiO-Ce are found  $2.72 \times 10^{-5}$ ,  $4.92 \times 10^{-5}$  and  $.08$  at 900 K respectively. It is very clear from the extracted data that from the above given condition NiO-Ce shows remarkable increment in figure of merit which is very favorable for our study and further investigation for renewable materials.

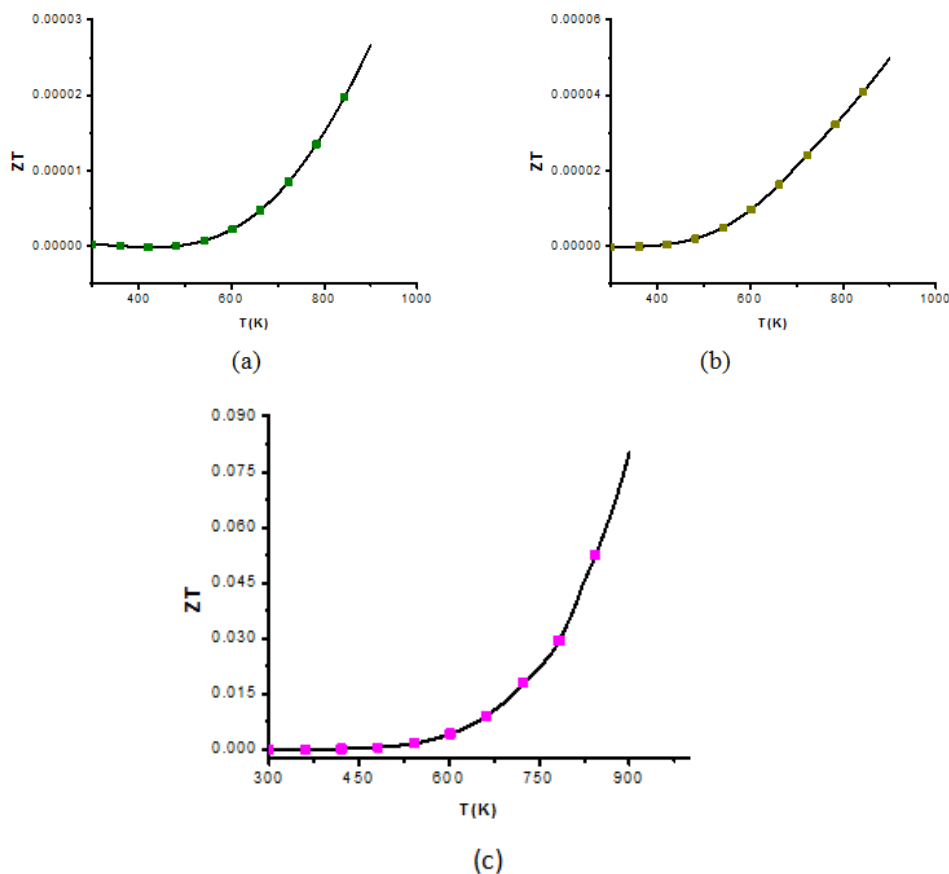


**Figure 8.** Figure of merit (ZT) Vs temperature graph of (a) Pure NiO (b) NiO-La (c) NiO-Ce.

**V. Conclusions**

The rare earth doped Nickel oxide nanoparticles (NiO-La & NiO-Ce) show the variation in their crystallinity and thermal stability due to doping. Doping also influence the transition temperature and calcinations temperature by which crystalline size also get affected. While analyzing the TGA curves it is concluded that the after doping Lanthanum in NiO there is 17 % weight loss and NiO-Ce shows weight gain but with instability in thermo-grams while the pure NiO is very much stable with respect to temperature. All the three samples posses same crystallization temperature at 433<sup>0</sup>C. Pure NiO and NiO-Ce has the sufficient purge process and the melting process were start near the onset temperature in both the material while NiO-La shows different characteristics in which a maximum weight loss is observed. The TGA and DSC curve are in agreement for all three samples and provide the significant information about thermal properties of the pure NiO, and NiO-La & NiO-Ce nanoparticles. Further more advanced and desirable study such as thermal conductivity, electrical conductivity, Seebeck coefficient and figure of merit samples gives the favorable results as we concluded that NiO-La is not suitable for thermoelectric application because it has very low ZT on the other hand Cerium doping gives the remarkable enhancement in the ZT in comparison with the pure NiO and NiO-La. The value of ZT of pure NiO and NiO-La & NiO-Ce nanoparticles are  $2.72 \times 10^{-5}$ ,  $4.92 \times 10^{-5}$  &  $.08$  at **900K** respectively. It is very clear that NiO-Ce nanoparticles are the better candidate for thermoelectric

applications at high temperature in air atmosphere due to high stability, low cost and high figure of merit. Thus for the thermoelectric properties optimization cerium element gives the favorable results in the given temperature range and hence it can be used as *p-type* leg in thermoelectric devices.

### Acknowledgments

The authors acknowledge the MPCST, Bhopal for their financial assistance and also extended the heartfelt gratitude to the staff of TPD, BARC, Mumbai for their guidance and providing characterization facilities LFA (Thermal conductivity), LSR (Seebeck coefficient) and FTIR. I also thankful to Central Instrument facility center, IISER, BHOPAL for characterization.

### References

- [1]. S. Walia, S. Balendhran, H. Nili Ahmadabadi, S. Zhuiykov, G. Rosengarten, Q. Wang, M. Bhaskaran, S. Sriram, M. Strano and K. Kalantar Zadeh, 2013. Transition metal oxides – Thermoelectric properties. *Progress in Materials Science*, 58(8), pp1443-1489.
- [2]. Y.W. Huang, C.H. Wu and R.S. Aronstam, 2010 Toxicity of Transition Metal Oxide Nanoparticles: Recent Insights from *in vitro* Studies, *Materials (Basel)* 3(10), pp 4842–4859
- [3]. M.M. Ba-Abbad, P.V. Chai, M.S. Takriff, A. Benamor and A.W. Mohammad, 2015 Optimization of nickel oxide nanoparticle synthesis through the sol-gel method using Box-Behnken design. *Material Design* 86, pp 948-956
- [4]. M.F. Garcia and J.A. Rodriguez, 2009 Nanomaterials: Inorganic and Bioinorganic Perspectives BNL-79479-2007-BC DOI: 10.1002/0470862106.ia377
- [5]. S. Barana, A. Hoserb, B. Penca and A. Szytuła, 2016 Size Effects in Antiferromagnetic NiO Nanoparticles *Acta Physica Polonica A* 129, 35-39
- [6]. A. Vanaja and K.S. Rao, 2016 Effect of Co Doping on Structural and Optical Properties of Zinc Oxide Nanoparticles Synthesized by Sol-Gel Method. *Advanced Nanoparticles*, 5(01), pp 83-89
- [7]. F.T. Thema, E. Manikandan, A. Gurib-Fakim and M. Maaza, 2016 Single phase Bunsenite NiO nanoparticles green synthesis by Agathosma betulina natural extract. *Journal of Alloys and Compounds*, 657, pp 655-661
- [8]. S.S.P. Sultana, D.H.V. Kishore, M. Kuniyil, M. Khan, A. Alwarthan, K.R.S. Prasad, J.P. Labis and S.F. Adil, 2015 Ceria doped mixed metal oxide nanoparticles as oxidation catalysts: Synthesis and their characterization. *Arabian Journal of Chemistry* 8, pp766-770
- [9]. M. Niederberger, 2007 Nonaqueous Sol-Gel Routes to Metal Oxide Nanoparticles. *Accounts of Chemical Research* 40(9), pp793-800
- [10]. S. Cotton, *Inorganic Chemistry*, 2006 A Wiley Series of Advanced Textbooks ISBN: 978-0-470-01006-8, pp1-280
- [11]. J. Rudy, M. Konings, O. Beneš, A. Kovács, D. Manara, D. Sedmidubský, Lev Gorokhov, V.S. Iorish, V. Yungman, E. Shenyavskaya, and E. Osina, 2014 The Thermodynamic Properties of the f-Elements and their Compounds. Part 2. The Lanthanide and Actinide Oxides. *Journal of Physical and Chemical Reference Data* 43(1)
- [12]. B.M. Abu-Zied, S. M. Bawaked, S.A. Kosa and W. Schwioger, 2016 Effect of Some Rare Earth Oxides Doping on the Morphology, Crystallite Size, Electrical Conductivity and N<sub>2</sub>O Decomposition Activity of CuO Catalyst. *International Journal of Electrochemical Science*, 11, pp 1568-1580
- [13]. D. Sridevi and K.V. Rajendran, 2010 Enhanced optical properties La doped ZnO nanoparticles *Advanced Materials Rapid communication* 4(10), pp1591-1593
- [14]. K.H. Ng, S. Lidiyawati, M.R. Somalu, A. Muchtar and H.A. Rahman, 2016 Influence of Calcination on the Properties of Nickel Oxide- Samarium Doped Ceria Carbonate (NiO-SDCC) Composite Anodes. *Procedia Chemistry* 19, pp267-274
- [15]. N. Sultaniadis and A.R. Barron, 2009 TGA/DSC-FTIR Characterization of Oxide Nanoparticles <http://cnx.org/content/m23038/1.2/OpenStax-CNX module: m23038, 1>
- [16]. J.Z. Wen, S. Ringuette, G. Bohlouli-Zanjani, A. Hu, N. Ha Nguyen and J. Persic, 2013 Characterization of thermochemical properties of Al nanoparticle and NiO nanowire composites *Nanoscale Research Letters*, 8, pp 184-197
- [17]. L. Zhang, P. Xiao, L. Shi, G. Henkelman, J.B. Goodenough and J. Zhou, 2015 Suppressing the bipolar contribution to the thermoelectric properties of Mg<sub>2</sub>Si<sub>0.4</sub>Sn<sub>0.6</sub> by Ge substitution *Journal of Applied Physics*, 117(15), pp 155103-155114
- [18]. P. Shahi, D.J. Singh, J.P. Sun, L.X. Zhao, G.F. Chen, J.Q. Yan, D.G. Mandrus and J.G. Chen, 2018 Bipolar Conduction as the Origin of the Electronic Transition in Pentatellurides: Metallic vs. Semiconducting Behavior. *Physics Review X* 8, pp 021055-021079
- [19]. S. Wang, J. Yang, T. Toll, J. Yang, W. Zhang and X. Tang, 2015 Conductivity-limiting bipolar thermal conductivity in semiconductors. *Scientific reports*, Pp 1-10 doi: 10.1038/srep10136.
- [20]. Y. Feng, X. Jiang, E. Ghafari, B. Kucukgok, C. Zhang, I. Ferguson and N. Lu, 2018 Metal oxides for thermoelectric power generation and beyond. *Advanced Compounds of Hybrid Materials* 1, pp 114-126
- [21]. A. Shaheen, W. Zia and M.S. Anwar, 2010 Band Structure and Electrical Conductivity in Semiconductors LUMS School of Science and Engineering
- [22]. E.B. Lavik and Y.M. Chiang, 2011 Electrical Conductivity of Pure and Doped Nanocrystalline Cerium Oxide 457 Symposium V – Nanophase and Nanocomposite Mater. II,

Characterization of thermochemical properties of Al nanoparticle and NiO nanowire composites

John Z Wen

1\*

, Sophie Ringuette

2

, Golnaz Bohlouli-Zanjani

1

, Anming Hu

1  
, Ngoc Ha Nguyen  
3  
, John Persic  
4  
,  
Catalin F Petre  
2  
and Y Norman Zhou

Characterization of thermochemical properties of  
Al nanoparticle and NiO nanowire composites

John Z Wen

1\*  
, Sophie Ringuette  
2  
, Golnaz Bohlouli-Zanjani

1  
, Anming Hu

1  
, Ngoc Ha Nguyen

3  
, John Persic

4  
,  
Catalin F Petre

2  
and Y Norman

IOSR Journal of Applied Physics (IOSR-JAP) is UGC approved Journal with SI. No. 5010,  
Journal no. 49054.

Smita Jain " Analysis of Thermoelectric Properties of Light Rare earth (La, Ce) Doped Nickel  
oxide Nanoparticles." IOSR Journal of Applied Physics (IOSR-JAP) , vol. 11, no. 2, 2019, pp.  
75-85.